Available online at www.sciencedirect.com
SCIENCE DIRECT
ELSEVIER
International Journal of Mass Spectrometry 251 (2006) 119–124
International Journal of Mass Spectrometry
www.elsevier.com/locate/ijms

Opportunistic mass measurements at the Holifield Radioactive Ion Beam Facility

P.A. Hausladen [a,*], J.R. Beene [a], A. Galindo-Uribarri [a], Y. Larochelle [b], J.F. Liang [a], P.E. Mueller [a], D. Shapira [a], D.W. Stracener [a], J. Thomas [c], R.L. Varner [a], H. Wollnik [a]

[a] *Physics Division, Oak Ridge National Laboratory, Oak Ridge, TN 37831, USA*
[b] *Department of Physics, University of Tennessee, Knoxville, TN 37996, USA*
[c] *Department of Physics and Astronomy, Rutgers University, Piscataway, NJ 08854, USA*

Received 30 September 2005; received in revised form 5 January 2006; accepted 9 January 2006
Available online 13 February 2006

Abstract

A technique for measuring mass differences has been developed at the Holifield Radioactive Ion Beam Facility (HRIBF) that requires no specialized equipment. Mass differences are measured as position differences between known and unknown-mass isobars, dispersed at the image of the energy-analyzing magnet following the 25 MV tandem post-accelerator, and identified by an energy-loss measurement. The technique has been demonstrated on neutron-rich $^{77–79}$Cu and $^{83–86}$Ge isotopes produced using the isotope separator online (ISOL) method with the ^{238}U(p,fission) reaction, where a mass accuracy of 500 keV was achieved. These nuclides are well suited to the measurement technique, as they readily migrate out of the production target and to the ion source and comprise the most neutron-rich elements of the isobarically mixed beam. Because modest precision mass values can be obtained with only a few tens of counts of the nuclide of interest among orders of magnitude more of the isobaric neighbors closer to stability, the sensitivity of this technique makes it appropriate for initial mass measurements far from stability.

PACS: 21.10.Dr; 29.30.−h; 07.75.+h

Keywords: Nuclear masses; Radioactive ion beams

1. Introduction

Systematic knowledge of nuclear masses underlies much of our understanding of nuclear matter, from its incompressibility and finite size, to the existence of shell structure and the possibility for "islands of stability" in the binding of super-heavy nuclei. This knowledge also underlies much of our understanding of the abundance of elements in nature. Yet, it is still not possible to understand the mass of complex nuclei in terms of the actual forces between nucleons. Consequently, masses are calculated by a variety of phenomenological approaches guided by attributes of the nucleon–nucleon interaction. While many of these approaches give comparable fits to known mass data, they can extrapolate quite differently out to the neutron drip line. Refinement of these methods will come principally from the measurement of new mass data. In this regard, points in the vicinity of closed and doubly-closed shells, giving the magnitude of shell effects where they are maximally manifest, and points far from stability, directly confirming the correct extrapolation toward the drip-lines, are of particular importance.

In general, new mass data far from stability come only as a result of considerable investment of resources in order to overcome the prodigious difficulties inherent in these measurements, including vanishing production, vanishing signal to background and, because of shrinking lifetimes, the vanishing time scale on which measurements must be made. The Holifield Radioactive Ion Beam Facility (HRIBF) produces a variety of neutron-rich beams of fission fragments from proton-induced fission of ^{238}U in a refractory UC_2 target, from which fission fragments are evolved, ionized, and post-accelerated in the 25 MV tandem accelerator. A small fraction of the fission yield in the mass 80 region stretches to the vicinity of doubly-magic ^{78}Ni. Recently,

* Corresponding author at: Bldg. 3500, MS-6010, Nuclear Science and Technology Division, Oak Ridge National Laboratory, Oak Ridge, TN 37831, USA. Tel.: +1 865 574 0284; fax: +1 865 576 8380.
E-mail address: hausladenpa@ornl.gov (P.A. Hausladen).

1387-3806/$ – see front matter © 2006 Elsevier B.V. All rights reserved.
doi:10.1016/j.ijms.2006.01.020

it was realized that mass measurements with modest mass accuracy sufficient to tell gross shell structure could be performed at the HRIBF with no specialized equipment [1]. The idea behind these measurements is simply that, after post-acceleration, the components of the isobarically mixed beam are dispersed at the focal plane of an analyzing magnet in proportion to their mass differences. A high resolution measurement of the position combined with unambiguous determination of the atomic number of each ion is then sufficient to measure the mass differences between unknown and known mass components of the beam. In this way, the characteristics of the HRIBF beams, that is, electrostatically accelerated and isobarically mixed, are used to maximum advantage: accelerated beam allows unambiguous determination of atomic number, isobarically mixed beam includes known mass differences as natural calibration points, and the momentum differences measured by the analyzing magnet originating in mass difference is a consequence of the mass independence of electrostatic acceleration. The purpose of the present work was to evaluate the efficacy of this technique by measuring the masses of nuclides reaching as neutron-rich as possible in the vicinity of doubly-magic ^{78}Ni.

2. Experiment

Suitable candidates for first measurements were identified by their ease of identification in a ΔE measurement and by the likelihood that short-lived, unknown mass isotopes would be able to migrate out of the target and to the ion source in sufficient number before decaying. The Cu isotopes, one proton from the closed-shell Ni isotopes, evolve from the target and to the ion source in times comparable to noble gases, while the nonexistence of the negative Zn ion makes identification of Cu in the ion chamber robust with $\Delta Z = 2$ to the nearest isobar. The Ge isotopes also readily evolve from the production target. Moreover, this element can be chemically selected by ionizing the GeS molecule, which migrates to the ion source more quickly, and is subsequently broken up on charge exchange [2]. Consequently, the Cu and Ge isotopes were chosen for proof of principle measurements.

For the measurements of heavy Cu isotopes, fissions of ^{238}U in a uranium carbide target were induced by 10 μA of 42 MeV protons from the Oak Ridge isochronous cyclotron (ORIC). Fission fragments evolved from the target from a combination of beam and external heating, were positively ionized in an electron beam plasma ion source, selected by mass number, charge exchanged, and isobarically purified in the nominally $M/\Delta M = 20{,}000$ low energy isobar separator. This purified beam was injected into the tandem accelerator and measured ion-by-ion near the focus of the analyzing magnet, where detectors to measure position and Z were installed as close as possible to the image of the $\rho = 1.67$ m bending-radius analyzing magnet of the 25 MV tandem accelerator. The layout of the facility, along with the major components used in the present work, is shown schematically in Fig. 1.

The analyzing magnet is located in a beam line which can be rotated to direct beam to different target areas. To accommodate

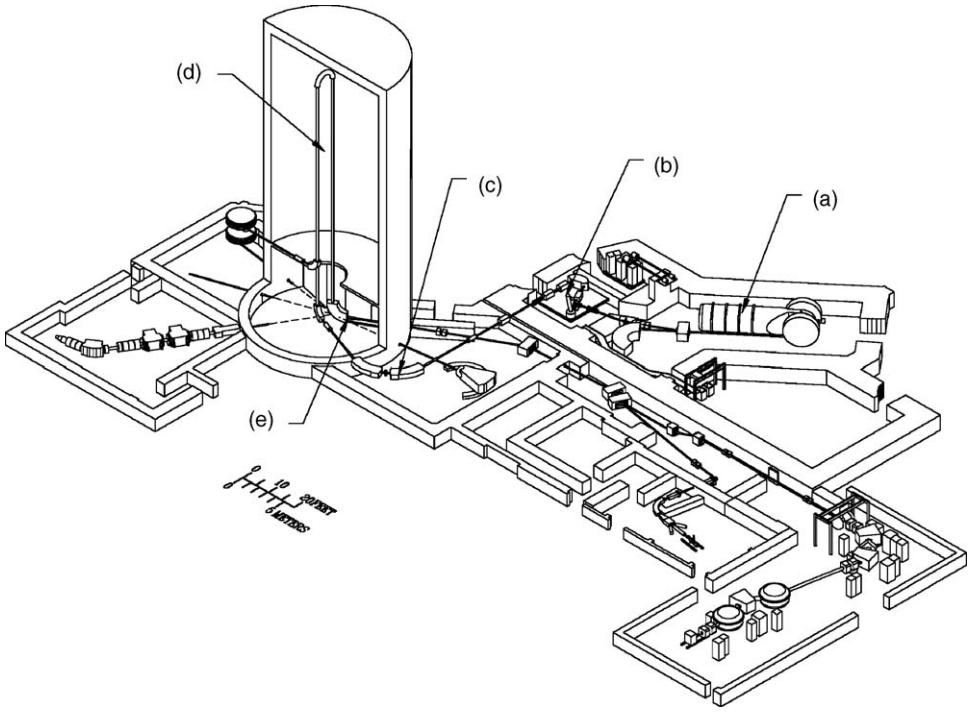

Fig. 1. The schematic layout of the Holifield Radioactive Ion Beam Facility (HRIBF), showing (a) the Oak Ridge isochronous cyclotron (ORIC), (b) the high voltage radioactive ion beam (RIB) production platform, (c) the isobar separator, (d) the 25 MV tandem post-accelerator, and (e) the energy-analyzing magnet. Protons from ORIC are directed to the uranium carbide target on the RIB platform where the induced fission fragments are evolved, positively ionized, separated by mass number and charge-exchanged to make negative ions suitable for injection into the tandem. Mass measurements were performed at the image of the energy-analyzing magnet following the tandem post-accelerator.

the new detectors, the magnet was rotated to a position where no beam line is presently in place. The position measurement was performed by means of a position-sensitive micro-channel plate (MCP) detector with four-corner resistive readout to determine the position of each ion that passed through the aluminized Mylar conversion dynode on its way to an ionization chamber. The position detector was modified from its implementation in other experiments by changing the angle of the foil so that it was inclined only 20° with respect to the beam direction rather than the usual 45° [3,4]. This change further spread displacements in the bending plane along the surface of the foil and accommodated addition of a second permanent magnet to the detector to further constrain the orbits of electrons traveling from the foil to the MCP. The Z measurement was performed by a Bragg-style or axial ion chamber, which was fabricated with a minimum of parts and time from a section of discarded acceleration tube to fit in the limited space available between the position detector and the wall of the magnet room. The MCP and ion chamber were assembled in a six-way cross. The MCP and ion chamber setup are shown schematically in Fig. 2. The resolution achieved for displacements in the bending plane of the analyzing magnet was 0.08 mm, measured by its response to a grid of 0.02 mm Au-plated W wires spaced (in the bending plane) by 0.33 mm. An image of this grid taken by the detector can be seen in Fig. 2. Performance of the ionization chamber was excellent, aided by the fast electron drift velocity of CF_4 gas and the addition of a range measurement consisting of the time difference between the MCP and the anode of the ion chamber. Fig. 2 also shows a plot of E versus range of the $A = 78$ isobars, where Cu appears with the longest range by virtue of its lower Z, and highest energy since it lost the least energy in the MCP foil and window to the ion chamber. For each ion, the four corners of the position-sensitive MCP, E, and ΔE in the ion chamber, the time difference between the MCP and ion chamber, and a microsecond time stamp were recorded.

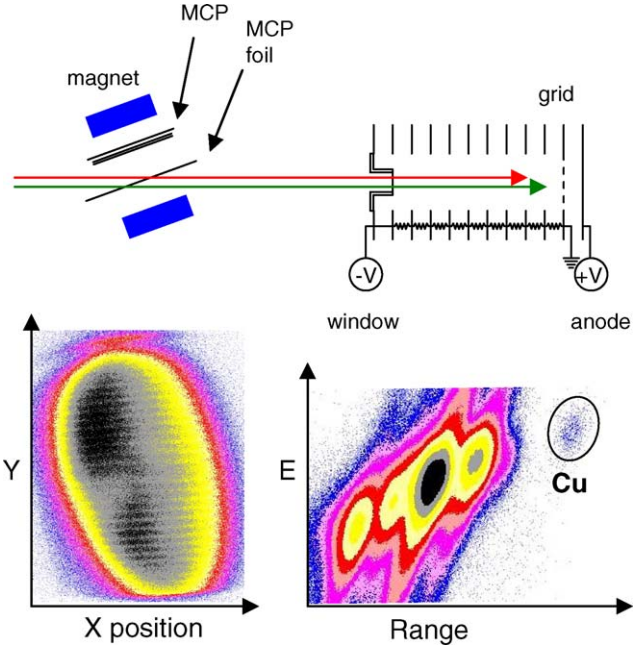

Fig. 2. Above, a schematic diagram of the position sensitive MCP and ion chamber used in the mass measurements is shown. Below, the position response of the MCP to a 0.02 mm wire grid placed over the MCP foil is shown, along with the response of the ion chamber to $A = 78$ isobars including $T_{1/2} = 0.3$ s ^{78}Cu. The position signals in the MCP were constructed from four-corner readout from a resistive anode. The range signal in the ion chamber is measured as the time difference between the MCP and the ion chamber anode.

The 25 MV tandem accelerator and detectors were initially set up with a mixed beam composed of ^{76}Se and ^{76}Ge from the stable injector. A terminal voltage of 22 MV was used to ensure stable operation, and dilute gas stripping was used to minimize emittance of the beam, necessitated by the location of the position measurement at a distance of 0.65ρ beyond the focus of the magnet. Charge state 9+ was selected at the terminal of the tandem as the highest possible with adequate yield for a final energy of 220 MeV or 2.9 MeV/A at which energy robust Z determination is possible. Much more than the ordinary care was taken in ensuring that the orbit through the analyzing magnet was known precisely. In order to accomplish this, the emittance and image slits located at ρ and 2ρ, respectively, following the magnet were sequentially narrowed and the trajectory retuned to maximize transmission through the slits. At this point, the object slits were closed down to 0.2 mm in the bending plane and the emittance and image slits opened larger than the 13 mm diameter acceptance of the ionization chamber. Under these conditions, the object slits transmitted approximately one quarter of the incident beam. The stable mixed-Z beam allowed the pressure and voltage of the ionization chamber to be adjusted for optimum Z separation, and the position response of the MCP to be calibrated by the 2.039 MeV mass difference between the two isobars.

The low energy separator was initially tuned with narrow object and image slit settings and centered on the most abundant isobar. The magnet field was then changed to make the expected mass of the Cu isotope the central trajectory, whereupon the object slits were opened to the nominal beam size and one slit edge was left in at the image to reduce the overall rate of known-mass isobars from approximately 5×10^6 s^{-1} to a manageable rate of about 5000 s^{-1} in the ion chamber. In this way, measurements of ^{76}Cu were performed, and measurements of $^{77–79}$Cu followed by scaling the magnetic elements of the beam transport appropriately. A mistakenly set gain on one of the MCP corners was discovered during the ^{77}Cu measurement that unfortunately meant that the ^{76}Cu data had to be discarded. It is worth noting, perhaps not surprisingly, that target heating is crucial to efficient extraction, particularly for the short-lived Cu isotopes. However, the magnitude of the effect is surprising in that a 25% drop in cyclotron current could make the measured Cu rate drop more than an order of magnitude.

For the measurements of Ge isotopes, additional considerations arose due to the consequences of chemical purification. The purification is accomplished by selecting the mass $A + 32$ beam out of the ion source, which selects the fraction of mass A isobars that form sulfide molecular ions (preferentially Ge). The molecules are then broken apart during the charge-exchange process and subsequent ion transport selects mass A. This purification reduces the quantity of non-Ge mass A isobars by orders

of magnitude. Because it is undesirable to further reduce the rate of calibrating masses, and because the momentum spread of Coulomb-exploded beam is converted to a spread in space by the isobar separator (thereby reducing transmission of the beam), dispersion of the separator was minimized by tuning a waist near its center. Since the additional role of the charge exchange cell in breaking up molecules favored a denser cell for maximum transmission of Ge isotopes, the cell was operated as hot as possible. Under these conditions, measurements were performed for $^{82–86}$Ge. Additional calibrating measurements for lighter Ge isotopes were not possible by this method because the calibrating masses did not show up with sufficient intensity. It is interesting to note that the amount of Ge, not just the fraction, is enhanced for the shorter lived isotopes of Ge because the GeS molecule is transported out of the target and to the ion source faster than Ge. In spite of this advantage, measurements were still extremely difficult by virtue of the very small total rate on the detector, in some cases one count every few seconds, making tuning adjustments difficult or impossible.

3. Analysis

For each mass measurement, the displacements at the focus of the magnet are given by $\Delta y = 2\rho(\Delta M/M + \Delta E/E)$, where the $\Delta M/M$ term is the dispersion in mass, and the $\Delta E/E$ term is common to all the isobars originating in voltage fluctuations of the terminal of the tandem accelerator. These fluctuations consist of a periodic component with a period of 1.2 s and a magnitude of 5×10^{-5}, and stochastic drifts that accumulate in magnitude over tens of minutes or hours. In order to account for these, the centroid of the position of the dominant isobar was tracked, and its rolling average for 100 events subtracted from the position determined for each ion. The amount of time required to accumulate the 100 events made it possible to remove both the periodic and stochastic drifts in terminal voltage for measurements with a high rate of calibrating masses, but only the stochastic drifts for measurements with a low rate of calibrating masses. Following this correction, the Gaussian width of a single-mass peak was 3 MeV, corresponding to a beam waist (FWHM) of 0.33 mm.

These mass measurements depend on highly accurate position measurements. As an example, a shift of only 5 μm for a mass 80 measurement corresponds to a shift of 100 keV in mass. The position response of the detector was therefore calibrated as carefully as achievable at all positions with the mass difference of the stable pair, ^{76}Se and ^{76}Ge. This calibration was accomplished by turning off the focusing quadrupoles prior to the object slits of the analyzing magnet so that the beam was much larger than the acceptance of the slits. The beam that was transmitted to the image in any tenth of a second, over which time scale the terminal voltage is effectively constant, was therefore two images of the object slits separated by 2.039 MeV in mass. The accelerator voltage was then slowly changed until every position on the detector had accumulated sufficient counts to determine the local value of the dispersion. By keeping a rolling average of the bending-plane position of both the Ge and Se components of the beam for a narrowly-defined region of the central portion of the detector in the orthogonal direction, the dispersion was mapped out for a vertical stripe on the detector, and the calculated position corrected to yield uniform dispersion. The remainder of the detector was corrected by means of bilinear interpolation to ensure that the slit image at each location in the bending plane corresponded to a horizontal line. Data from the mass measurements were examined subsequent to the calibration to determine that position differences could vary by as much as 300 keV (15 μm) depending where on the detector they were measured.

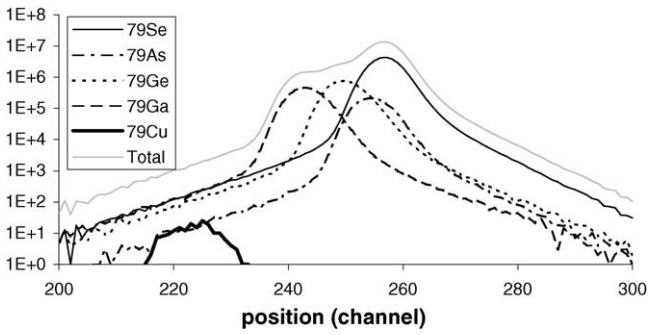

Fig. 3. Position measurement for $A = 79$ isobars. Identification of each isobar was performed in an ion chamber.

With these corrected data, the position spectrum of each isobar was accumulated over the course of the run. In order to ensure that there was no significant misidentification of isobars in the ion chamber, restrictive conditions were placed on the $E\,\Delta E$ and E-range data for calibrating masses so that only about a third of the total counts were considered positively identified. An example of the position data for the $A = 79$ measurement of ^{79}Cu are shown in Fig. 3, in which the position differences can be seen to be proportional to mass difference. It is clear that the ^{79}Cu counts contain no misidentified counts of other isobars despite themselves not being visible in the total spectrum. The centroids of these data, scaled by $1/A$, were combined with the $A = 77$ and 78 data and the known mass excesses Δ, and fit to a common line to determine the correct mass calibration for these data. Since the absolute position of each data set is not known, one was fixed, and the remaining two were allowed to be offset in finding the best fit. In the cases where there are known isomeric states for the calibration masses, the known mass was taken to be the average of the ground and isomeric states and the uncertainty increased accordingly. The result of this fit for the Cu measurements can be seen in Fig. 4(a), where the scatter of points about the fit is slightly less than the 300 keV uncertainty in the determination of the positions noted above. The prescription was repeated separately for the Ge measurements, and is shown in Fig. 4(b). Interestingly, the scatter in the points about the fit for the longer measurements was less, apparently a consequence of averaging out local nonlinearities in the response of the MCP (originating in small ripples in the aluminized Mylar foil and inhomogeneities in the resistive anode inadequately accounted for by the calibration) as terminal voltage drifts sampled different parts of the detector. Results of the extrapolation to unknown mass excesses for $^{77–79}$Cu and $^{83–86}$Ge are shown in Table 1, along with their known half-lives and measured count rates at

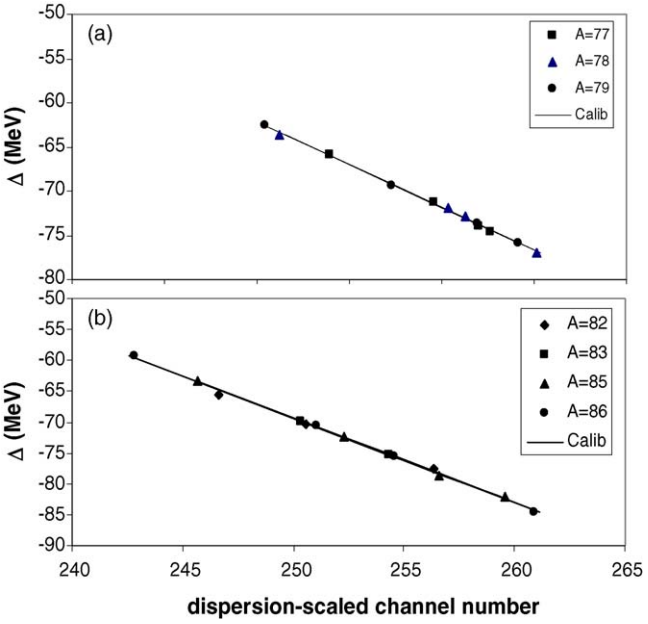

Fig. 4. Calibration masses vs. dispersion-scaled channel for (a) Cu measurements and (b) Ge measurements. The values of reduced χ^2 for the fits are 0.83 and 0.82, respectively, indicating that the estimated 300 keV systematic uncertainty in the position measurements is close to the actual value.

Table 1
Measured mass excesses and detected count rates of Cu and Ge isotopes

Nuclide	Mass excess (MeV)	$T_{1/2}$ (s)	Count rate at detector (s^{-1})
^{77}Cu	−48.3 (5)	0.469 (8)	2
^{78}Cu	−44.5 (5)	0.342 (11)	0.15
^{79}Cu	−43.5 (5)	0.188 (12)	0.006
^{83}Ge	−60.8 (3)	1.85 (6)	1500
^{84}Ge	−58.0 (4)	0.947 (11)	95
^{84}As	−75.7 (3)	3.24 (26)	100
^{85}Ge	−53.3 (5)	0.535 (47)	1.3
^{86}Ge	−51.0 (5)	0.2 (syst)	0.006

The rates of positive ions from the ion source prior to charge exchange and transmission through the tandem post-accelerator and mass analyzing magnet is greater by a factor of about 150.

the detector. A mass excess for the nuclide ^{84}As can also be obtained from the data and is correspondingly shown in Table 1. The calibrating masses were taken from Ref. [5] with the exception of the values for ^{85,86}As, which were taken from Ref. [6]. Those measurements for which the mass was interpolated and the statistical error was small are reported with the 300 keV systematic uncertainty in the determination of positions. More typically, the statistical uncertainty and error in the extrapolation of the calibration curves shown in Fig. 4 combined to yield an error of about 500 keV.

4. Discussion

Competition between the quenching of the $N = 50$ neutron shell gap with decreasing Z and mutually enhanced magicity in the $Z = 28$ region combine to make the evolution of this shell gap a fertile testing ground for the development of mass calculations.

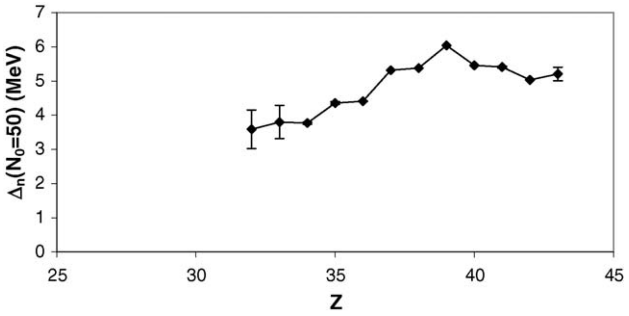

Fig. 5. Calculated $N_0 = 50$ shell gaps as a function of proton number. Data for the points from $Z = 34$ to 43 are from the most recent mass evaluation [5], while data for $Z = 33$ are from Ref. [6], and data for $Z = 32$ are from the present work.

Unfortunately, direct measurement of the neutron shell gap at $Z = 28$ will require measurement of the masses of ^{76,78,80}Ni. For comparison, in the most recent mass evaluation [5], the lowest Z for which the neutron gap can be calculated from measured masses is 34. Measurements from GSI add $Z = 33$ [6], and the present work adds $Z = 32$. The shell gap $\Delta_n(N_0, Z) = S_{2n}(N_0, Z) - S_{2n}(N_0 + 2, Z)$ is shown in Fig. 5 for those elements where it can be calculated from measured data, and it shows no evidence at $Z = 32$ of an upswing towards a maximum at $Z = 28$. Considering the large error bars of the new points, the upswing would have to be dramatic to be detectable.

While the Cu measurements do not permit calculation of Δ_n, inspection of the S_{2n} may give clues to whether the $N_0 = 50$ shell gap at $Z = 29$ is enhanced. For this purpose, the measured S_{2n} values for evaluated masses and the present work have been compared to microscopic calculations by Duflo and Zuker [7] and Goriely et al. [8]. The mass formula of Duflo and Zuker provides the best global fit to known masses, in part because it reproduces the mutually enhanced magicity for $N_0 = 82$ and $N_0 = 126$, although it fails to reproduce either the mutually enhanced magicity near $Z = 40$ or the quenching of the shell gap for larger neutron excesses at $N_0 = 50$. The Hartree–Fock calculations of Goriely incorporate a pairing-cutoff prescription that reproduces the quenching of the $N_0 = 50$ shell gap for larger neutron excesses, but like other Hartree–Fock calculations, under-binds the doubly-magic nuclei ^{48}Ca, ^{132}Sn, and ^{208}Pb, as well as their immediate neighbors [9]. In Fig. 6, the measured S_{2n} values for evaluated masses and the present work are shown for the isotopes of Cu, Zn, Ga, and Ge, along with microscopic calculations by Duflo and Zuker (labeled DuZu) and Goriely (labeled HFB-2). In order to accentuate differences, the data and calculations are plotted with the HFB-2 values subtracted from them. The HFB-2 formula appears to correctly predict the magnitude of masses in the vicinity of the $N_0 = 50$ shell gap for $Z = 30$–32. The mass formula of Duflo and Zuker over-predicts the masses at and just before the $N_0 = 50$ shell gap for $Z = 30$–32, a consequence of a shell gap for this region that is stronger by almost a factor of 2 than HFB-2. Interestingly, the new experimental data for the Cu isotopes appear to follow the trend of Duflo and Zuker, perhaps an initial indication of increased binding due to mutually enhanced magicity at doubly-magic ^{78}Ni.

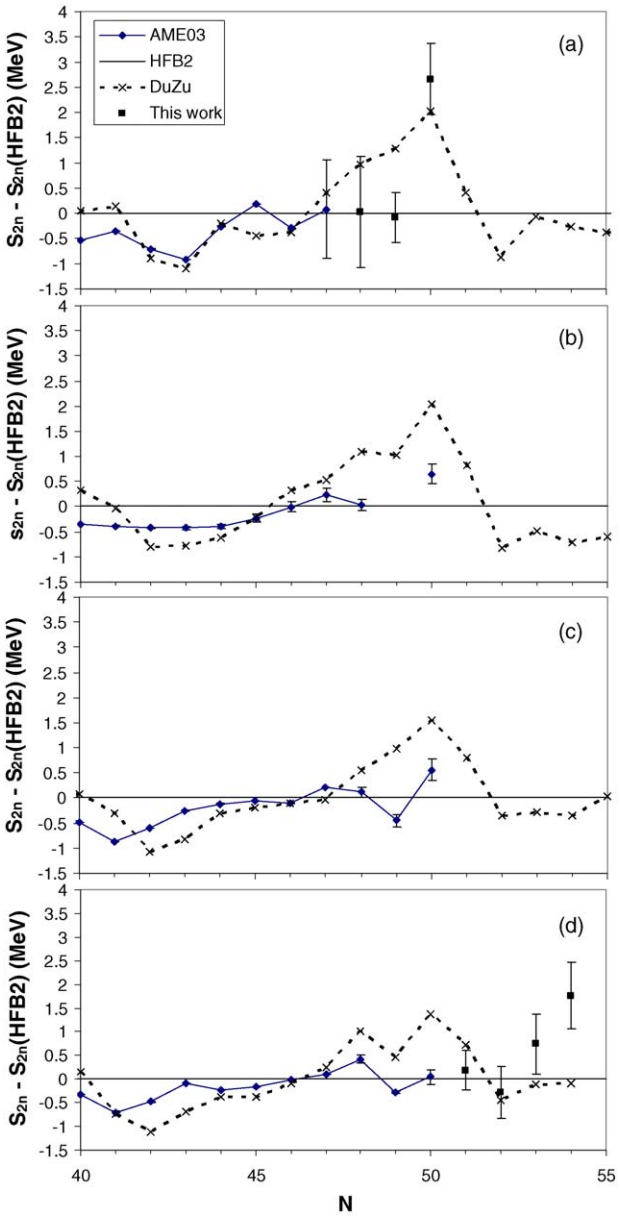

Fig. 6. Model-subtracted two-neutron separation energies S_{2n}–S_{2n} (HFB-2) of experiment, the Hartree–Fock mass formula HFB-2, and the formalism of Duflo and Zuker for (a) the Cu isotopes, (b) the Zn isotopes, (c) the Ga isotopes, and (d) the Ge isotopes. Because the values for the Hartree–Fock mass formula HFB-2 have been subtracted, the HFB-2 points define the axis.

5. Conclusions

The measurements described herein provide proof of principle of a simple technique of measuring masses that can measure short half-life nuclides far from stability with rates of the nuclide of interest as low as $20\,h^{-1}$. Despite a setup that was far from optimized, it yielded data of surprisingly high quality that may see the first indication of enhanced binding of ^{79}Cu. With modest effort, both systematic and statistical errors can be reduced substantially, particularly by moving the position measurement much closer to the magnet focus, but also by changing to a MCP foil such as silicon nitride which will not sag and wrinkle with use or handling. With such improvements, it would be possible to make measurements with even fewer counts, perhaps as low as 20 per day. Last of all, future measurements would be prudent to include as long a mass chain as possible to dramatically increase the number and footprint of calibrating masses to reduce extrapolation error and average out the systematic errors of each contributing point.

Acknowledgements

The authors gratefully acknowledge Carl Gross and Jeff Blackmon for invaluable contributions of equipment and advocacy, and the operations staff, especially Ray Juras and Martha Meigs, for tireless enthusiasm without which the present work would not have been possible. This research is supported by the US Department of Energy under contract No. DE-AC05-00OR22725 with UT-Battelle, LLC.

References

[1] P.A. Hausladen, J.R. Beene, A. Galindo-Uribarri, J.F. Liang, D.C. Radford, D. Shapira, Nucl. Instrum. Methods B 223–224 (2004) 176.
[2] D.W. Stracener, Nucl. Instrum. Methods B 204 (2003) 42.
[3] D. Shapira, T.A. Lewis, L.D. Hulett, Z. Ciao, Nucl. Instrum. Methods A 449 (2000) 396.
[4] D. Shapira, T.A. Lewis, L.D. Hulett, Nucl. Instrum. Methods A 454 (2000) 409.
[5] G. Audi, A.H. Wapstra, C. Thibault, Nucl. Phys. A 729 (2003) 337.
[6] M. Matos, unpublished Ph.D. thesis, University of Giessen, Giessen, Germany 2004.
[7] J. Duflo, A.P. Zuker, Phys. Rev. C 52 (1995) 23.
[8] S. Goriely, M. Samyn, P.-H. Heenen, J.M. Pearson, F. Tondeur, Nucl. Phys. C 66 (2002) 024326.
[9] D. Lunney, J.M. Pearson, C. Thibault, Rev. Mod. Phys. 75 (2003) 1021.